The Mo_2FeB_2- and Mn_2AlB_2-Type Modifications of RE_2Ni_2Cd (RE = La, Pr, Nd, Sm, Tb, Dy)

Thomas Fickenscher[a], Ute C. Rodewald[a], Dirk Niepmann[a], Ratikanta Mishra[b], Marcus Eschen[a], and Rainer Pöttgen[a]

[a] Institut für Anorganische und Analytische Chemie, Westfälische Wilhelms-Universität Münster, Corrensstraße 36, D-48149 Münster, Germany
[b] Applied Chemistry Division, Bhabha Atomic Research Centre, Trombay, Mumbai-400 085, India

Reprint requests to R. Pöttgen. E-mail: pottgen@uni-muenster.de

Z. Naturforsch. **60b,** 271 – 276 (2005); received December 3, 2004

The rare earth metal (RE)–nickel–cadmium intermetallics RE_2Ni_2Cd (RE = La, Pr, Nd, Sm, Tb, Dy) were prepared from the elements in sealed niobium or tantalum tubes in a water-cooled sample chamber of a high-frequency furnace. They crystallize with a tetragonal Mo_2FeB_2 type low-temperature modification, space group $P4/mbm$, and an orthorhombic Mn_2AlB_2 type high-temperature modification, space group $Cmmm$. The cadmium compounds were characterized through their X-ray powder patterns. Five structures of the low-temperature modifications were refined from X-ray single crystal diffractometer data: $a = 763.76(9)$, $c = 387.26(8)$ pm, wR2 = 0.046, 205 F^2 for $La_2Ni_{1.67(1)}Cd$; $a = 752.93(7)$, $c = 380.95(6)$ pm, wR2 = 0.061, 260 F^2 for Pr_2Ni_2Cd; $a = 750.88(9)$, $c = 378.33(7)$ pm, wR2 = 0.051, 195 F^2 for Nd_2Ni_2Cd; $a = 743.6(1)$, $c = 374.0(1)$ pm, wR2 = 0.036, 386 F^2 for $Sm_2Ni_{1.93(1)}Cd$; $a = 734.9(1)$, $c = 366.1(2)$ pm, wR2 = 0.030, 252 F^2 for $Dy_2Ni_{1.94(1)}Cd$, with 13(12) variables per refinement. The 4g nickel site is only fully occupied in the neodymium and the praseodymium compound. Both modifications can be considered as intergrowths of distorted AlB_2 and CsCl related slabs. In both modification the nickel and cadmium atoms build up two-dimensional $[Ni_2Cd]$ networks. In the low-temperature modifications the nickel atoms form pairs, while nickel zig-zag chains occur in the high-temperature modifications. These nickel fragments are condensed *via* the cadmium atoms. The crystal chemistry and the chemical bonding in these intermetallics is discussed.

Key words: Rare Earth Compounds, Cadmium, Phase Transition, Crystal Chemistry

Introduction

In continuation of our investigations on the structures and properties of Mo_2FeB_2 type intermetallics RE_2T_2X (RE = rare earth element, T = late transition metal, X = element of the 3rd or 4th main group) [1], we have recently substituted the X component also by magnesium and cadmium [2 – 11]. This move leads to reduced electron counts and thus influences the magnetic properties. To give an example, the Néel temperature increases from 5 K for Pr_2Pd_2In [12, 13] to 15 K for Pr_2Pd_2Mg [9]. Also homogeneity ranges occur that effect the magnetic behavior. $Ce_2Rh_{1.86}Cd$ [8] is an intermediate-valent system while cerium is tetravalent in Ce_2Rh_2In [14].

In the rare earth metal–nickel–cadmium systems, so far only mixed-valent $Ce_2Ni_{1.88}Cd$ [2] and the 65 K antiferromagnet Gd_2Ni_2Cd [15] have been reported. While the cerium compound adopts the tetragonal Mo_2FeB_2 structure (space group $P4/mbm$) [16], a ternary ordered version of U_3Si_2 [17, 18], Gd_2Ni_2Cd is isotypic with orthorhombic Mn_2AlB_2 [19], space group $Cmmm$. Both structure types are composed of similar AlB_2 and CsCl related slabs. Our recent phase analytical investigations in the rare earth metal–nickel–cadmium systems have revealed that some of the RE_2Ni_2Cd intermetallics with Mo_2FeB_2 structure have extended homogeneity ranges $RE_2Ni_{2-x}Cd$ and that some transform to an Mn_2AlB_2 type high-temperature modification. The synthesis and structural investigation of these RE_2Ni_2Cd intermetallics is reported herein.

Experimental Section

Synthesis

Starting materials for the preparation of the RE_2Ni_2Cd samples were ingots of the rare earth metals (Johnson

Matthey, Chempur or Kelpin), nickel wire (∅ 0.38 mm, Johnson-Matthey) or nickel powder (Johnson-Matthey), and a cadmium rod (Johnson Matthey, ∅ 8 mm), all with stated purities better than 99.9%. Pieces of the rare earth metal ingots, nickel wire or nickel powder and small pieces of the cadmium rod were weighed in the ideal 2:2:1 atomic ration and sealed in niobium or tantalum ampoules under an argon pressure of about 800 mbar [20]. The argon was purified over titanium sponge (900 K), silica gel, and molecular sieves. The high-melting metal tubes were placed in a water-cooled sample chamber [21] of an induction furnace (Hüttinger Elektronik, Freiburg, Typ TIG 5/300 or Kontron Roto-Melt 1.2 kW). Synthesis of the RE_2Ni_2Cd samples *via* arc-melting is not possible, due to the low boiling temperature (1040 K) of cadmium.

The metal ampoules were first rapidly heated at *ca.* 1520 K and held at that temperature for 2 min. The subsequent annealing procedures were carried out either directly in the sample chamber of the induction furnace or the tantalum tubes were sealed in evacuated quartz tubes and placed in muffle furnaces. The various samples were annealed between *ca.* 670 and *ca.* 1070 K for periods of 2 h in the induction coil and for 2 weeks in the muffle furnaces. The annealing procedures at the lowest temperatures revealed the tetragonal Mo_2FeB_2 compounds, while the orthorhombic Mn_2AlB_2 phases occurred at the higher annealing temperatures. The temperature control at the induction furnace was ensured through a Sensor Therm Metis MS09 pyrometer with an accuracy of ±30 K. The muffle furnaces were controlled through standard Ni–Cr/Ni thermocouples.

After the annealing procedures, all RE_2Ni_2Cd samples could be broken mechanically off the ampoule walls. No reactions with the crucible material could be detected. Compact pieces and powders of the RE_2Ni_2Cd compounds are stable in air over long periods of time. Powders are dark grey and the single crystals exhibit metallic lustre.

X-ray film data and structure refinements

The samples annealed at the various temperatures were characterized on a Stoe StadiP powder diffractometer (with silicon (a = 543.07 pm) as an external standard) or through Guinier powder patterns (α-quartz (a = 491.30, c = 540.46 pm) as an internal standard) using Cu-$K_{\alpha1}$ radiation. The Guinier camera was equipped with an imaging plate system (Fujifilm BAS–1800). The lattice parameters (Table 1) were obtained from least-squares fits of the X-ray powder data. The correct indexing was ensured through comparison with calculated patterns [22] using the atomic positions obtained from the structure refinements. The lattice parameters derived for the powders and the single crystals agreed well.

So far it was only possible to get small single crystals for the low-temperature modifications. Irregularly shaped single crystals of $La_2Ni_{1.67}Cd$, Pr_2Ni_2Cd, Nd_2Ni_2Cd, $Sm_2Ni_{1.93}Cd$, and $Dy_2Ni_{1.94}Cd$ were isolated from the annealed samples by mechanical fragmentation and examined by Laue photographs on a Buerger precession camera (equipped with an imaging plate system Fujifilm BAS–1800) in order to establish suitability for intensity data collection. Intensity data of $La_2Ni_{1.67}Cd$, Pr_2Ni_2Cd, Nd_2Ni_2Cd, and $Sm_2Ni_{1.93}Cd$ were collected at room temperature by use of a four-circle diffractometer (CAD4) with graphite monochromatized Mo-K_α radiation (71.073 pm) and a scintillation counter with pulse height discrimination. The scans were performed in the $\omega/2\theta$ mode. Empirical absorption corrections were applied on the basis of Ψ-scan data, followed by spherical absorption corrections. The $Dy_2Ni_{1.94}Cd$ crystal was investigated by use of a Stoe IPDS–II diffractometer with graphite monochromatized Mo-K_α radiation. The absorption correction for this crystal was numerical. All relevant crystallographic data for the data collections and evaluations are listed in Table 2.

Table 1. X-ray powder lattice parameters of the tetragonal low-temperature modifications with Mo_2FeB_2 type and the orthorhombic high-temperature modifications with Mn_2AlB_2 type of the intermetallic compounds RE_2Ni_2Cd.

Compound	a [pm]	b [pm]	c [pm]	V [nm^3]	Ref.
LT–La_2Ni_2Cd	763.76(9)	a	387.26(8)	0.2259	this work
LT–Ce_2Ni_2Cd	755.67(8)	a	375.14(6)	0.2142	[2]
LT–Pr_2Ni_2Cd	752.93(7)	a	380.95(6)	0.2160	this work
LT–Nd_2Ni_2Cd	750.88(9)	a	378.33(7)	0.2133	this work
LT–Sm_2Ni_2Cd	743.6(1)	a	374.0(1)	0.2068	this work
LT–Tb_2Ni_2Cd	736.69(9)	a	368.10(9)	0.1998	this work
LT–Dy_2Ni_2Cd	734.9(1)	a	366.1(2)	0.1977	this work
HT–La_2Ni_2Cd	406.2(4)	1470(1)	391.2(2)	0.2335	this work
HT–Sm_2Ni_2Cd	396.0(2)	1432.5(5)	374.9(2)	0.2126	this work
HT–Gd_2Ni_2Cd	393.90(3)	1423.57(9)	371.26(3)	0.2082	[15]
HT–Tb_2Ni_2Cd	393.0(1)	1420.5(4)	369.0(1)	0.2060	this work

The isotypism of the low-temperature modifications with the previously reported cerium compound $Ce_2Ni_{1.88}Cd$ [2] was already evident from the X-ray powder data. The atomic positions were taken as starting values and the structures were refined using SHELXL-97 (full-matrix least-squares on F_o^2) [23] with anisotropic atomic displacement parameters for all sites. As a check for the correct site assignment and possible nickel defects (see $Ce_2Ni_{1.88}Cd$ [2]), the occupancy parameters were refined in separate series of least-squares cycles. The rare earth and cadmium sites were fully occupied within one standard deviation for all crystals. Also the nickel sites in Pr_2Ni_2Cd and Nd_2Ni_2Cd were fully occupied, while there are small defects on the 4*g* nickel sites of the samarium and the dysprosium crystal and even larger defects for the lanthanum crystal, leading to the refined compositions $La_2Ni_{1.67}Cd$, $Sm_2Ni_{1.93}Cd$, and $Dy_2Ni_{1.94}Cd$. The nickel occupancy parameters for these crystals have been refined as a least-squares variable in the last cycles. Final difference Fourier syntheses revealed no significant residual peaks (see

Table 2. Crystal data and structure refinement for $La_2Ni_{1.67(1)}Cd$, Pr_2Ni_2Cd, Nd_2Ni_2Cd, $Sm_2Ni_{1.93(1)}Cd$, and $Dy_2Ni_{1.94(1)}Cd$ (Mo_2FeB_2 type, space group $P4/mbm$, $Z = 2$). The data collections were performed at room temperature.

Empirial formula	$La_2Ni_{1.67(1)}Cd$	Pr_2Ni_2Cd	Nd_2Ni_2Cd	$Sm_2Ni_{1.93(1)}Cd$	$Dy_2Ni_{1.94(1)}Cd$
Molar mass [g/mol]	487.68	511.64	518.30	530.52	554.82
Lattice parameters	Table 1	Table 1	Table 1	Table 1	Table 1
Calculated density [g/cm^3]	7.17	7.87	8.07	8.52	9.32
Crystal size [μm^3]	$15\times30\times40$	$15\times40\times60$	$10\times20\times25$	$20\times30\times50$	$8\times20\times50$
Transmission (max : min)	1.49	1.68	1.57	1.46	1.79
Absorption coefficient [mm^{-1}]	29.7	35.3	37.2	41.7	51.7
Detector distance [mm]	–	–	–	–	60
Exposure time [min]	–	–	–	–	12
ω Range; increment [°]	–	–	–	–	0 – 180; 1.0
Integr. param. A, B, EMS	–	–	–	–	14.0; 4.0; 0.014
$F(000)$	417	444	448	456	472
θ Range [°]	3 to 30	3 to 35	3 to 30	3 to 40	3 to 35
Range in hkl	$\pm10,\pm10,\pm5$	$\pm12,\pm12,+4$	$\pm10,\pm10,+5$	$\pm13,\pm13,\pm6$	$\pm11,\pm11,\pm5$
Total no. reflections	2418	1679	1309	4847	2701
Independent reflections	205 ($R_{int} = 0.078$)	260 ($R_{int} = 0.100$)	195 ($R_{int} = 0.089$)	386 ($R_{int} = 0.065$)	252 ($R_{int} = 0.078$)
Reflections with $I > 2\sigma(I)$	183 ($R_\sigma = 0.029$)	209 ($R_\sigma = 0.051$)	166 ($R_\sigma = 0.042$)	343 ($R_\sigma = 0.022$)	204 ($R_\sigma = 0.040$)
Data / parameters	205 / 13	260 / 12	195 / 12	386 / 13	252 / 13
Goodness-of-fit on F^2	1.023	1.040	1.185	1.087	0.984
Final R indices [$I > 2\sigma(I)$]	$R1 = 0.023$	$R1 = 0.035$	$R1 = 0.028$	$R1 = 0.018$	$R1 = 0.026$
	$wR2 = 0.045$	$wR2 = 0.057$	$wR2 = 0.046$	$wR2 = 0.034$	$wR2 = 0.029$
R Indices (all data)	$R1 = 0.029$	$R1 = 0.051$	$R1 = 0.045$	$R1 = 0.025$	$R1 = 0.038$
	$wR2 = 0.046$	$wR2 = 0.061$	$wR2 = 0.051$	$wR2 = 0.036$	$wR2 = 0.030$
Extinction coefficient	0.0049(8)	0.012(1)	0.030(2)	0.0024(4)	0.0075(6)
Largest diff. peak and hole [e/Å^3]	1.26 and −1.42	2.57 and −2.25	1.82 and −1.78	1.80 and −1.42	1.40 and −1.85

Table 3. Atomic coordinates and isotropic displacement parameters for $La_2Ni_{1.67(1)}Cd$, Pr_2Ni_2Cd, Nd_2Ni_2Cd, $Sm_2Ni_{1.93(1)}Cd$, and $Dy_2Ni_{1.94(1)}Cd$.

Atom	Wyckoff position	Occup.	x	y	z	U_{eq}[a]
$La_2Ni_{1.67(1)}Cd$						
La	4*h*	1.00	0.17663(5)	$1/2+x$	1/2	114(2)
Ni	4*g*	0.835(8)	0.3817(2)	$1/2+x$	0	178(6)
Cd	2*a*	1.00	0	0	0	154(3)
Pr_2Ni_2Cd						
Pr	4*h*	1.00	0.17634(6)	$1/2+x$	1/2	123(2)
Ni	4*g*	1.00	0.3816(2)	$1/2+x$	0	182(5)
Cd	2*a*	1.00	0	0	0	143(4)
Nd_2Ni_2Cd						
Nd	4*h*	1.00	0.17621(8)	$1/2+x$	1/2	127(3)
Ni	4*g*	1.00	0.3815(2)	$1/2+x$	0	195(5)
Cd	2*a*	1.00	0	0	0	154(4)
$Sm_2Ni_{1.93(1)}Cd$						
Sm	4*h*	1.00	0.17611(2)	$1/2+x$	1/2	89(1)
Ni	4*g*	0.965(4)	0.38138(7)	$1/2+x$	0	130(2)
Cd	2*a*	1.00	0	0	0	117(1)
$Dy_2Ni_{1.94(1)}Cd$						
Dy	4*h*	1.00	0.17370(4)	$1/2+x$	1/2	111(1)
Ni	4*g*	0.970(8)	0.3791(1)	$1/2+x$	0	144(5)
Cd	2*a*	1.00	0	0	0	124(2)

[a] U_{eq} (pm^2) is defined as one third of the trace of the orthogonalized U_{ij} tensor.

Table 4. Interatomic distances (pm) in the structures of LT-$Dy_2Ni_{1.94}Cd$ and HT-Gd_2Ni_2Cd. Standard deviations are equal or less than 0.2 pm. The data for the gadolinium compound were taken from ref. [15].

LT-$Dy_2Ni_{1.94}Cd$				**HT-Gd_2Ni_2Cd**			
Dy:	2	Ni	281.2	Gd:	4	Ni	285.2
	4	Ni	286.2		2	Ni	298.1
	4	Cd	327.6		4	Cd	333.2
	1	Dy	361.1		2	Gd	371.3
	2	Dy	366.1		2	Gd	378.4
	4	Dy	384.2		1	Gd	388.6
					2	Gd	393.9
Ni:	1	Ni	251.4	Ni:	2	Ni	243.5
	2	Dy	281.2		1	Cd	284.2
	4	Dy	286.2		4	Gd	285.2
	2	Cd	292.4		2	Gd	298.1
Cd:	4	Ni	292.4	Cd:	2	Ni	284.2
	8	Dy	327.6		8	Gd	333.2

Table 2). The positional parameters and interatomic distances are listed in Tables 3 and 4. Further details on the structure refinements are available*.

*Details may be obtained from: Fachinformationszentrum Karlsruhe, D-76344 Eggenstein-Leopoldshafen (Germany), by quoting the Registry No's. CSD 414595 ($La_2Ni_{1.67}Cd$), CSD 414596 (Pr_2Ni_2Cd), CSD 414597 (Nd_2Ni_2Cd), CSD 414598 ($Sm_2Ni_{1.93}Cd$), and CSD 414599 ($Dy_2Ni_{1.94}Cd$).

EDX analyses

The bulk samples and the single crystals measured on the diffractometers have been analyzed by EDX using a LEICA 420 I scanning electron microscope with the rare earth trifluorides, nickel, and cadmium as standards. The single crystals mounted on the quartz fibres were coated with a thin carbon film. Pieces of the bulk samples were polished with different silica and diamond pastes and left unetched for the analyses in the scanning electron microscope in backscattering mode. The EDX analyses revealed no impurity elements. For the bulk samples and the five single crystals the analyses were, within the experimental errors, all close to the ideal RE_2Ni_2Cd compositions.

Discussion

Synthesis conditions

So far, only the tetragonal, Mo_2FeB_2 type compounds RE_2Ni_2Cd and $RE_2Ni_{2-x}Cd$ were obtained in X-ray pure form. The samples prepared *via* the long-term annealing procedures at higher temperature always revealed the orthorhombic Mn_2AlB_2 type intermetallics RE_2Ni_2Cd as the major phase, but considerable degrees of the Mo_2FeB_2 type compounds still remained in these samples. Thus, the samples had not completely transformed to the orthorhombic modifications and consequently no phase pure synthesis of the orthorhombic RE_2Ni_2Cd intermetallics was yet possible. Unfortunately our Mn_2AlB_2 type crystals were not of sufficient quality for X-ray examinations. Our synthesis conditions could not be compared with those of Mn_2AlB_2 type Gd_2Ni_2Cd [15], since these authors did not report the annealing temperature.

Crystal chemistry

The family of RE_2Ni_2Cd (*RE* = La, Pr, Nd, Sm, Tb, Dy) intermetallics was investigated by X-ray diffraction on powders and single crystals. Similar to the series of indides $RE_2Ni_{2-x}In$ and RE_2Ni_2In [24, 25], for the RE_2Ni_2Cd intermetallics two different structure types also occur. The low-temperature modifications crystallize with the tetragonal Mo_2FeB_2 structure [16], while the high-temperature compounds adopt the orthorhombic Mn_2AlB_2 type [19]. However, there is one significant difference for the cadmium compounds described here. While the tetragonal indides show all defects on the nickel site, for tetragonal Pr_2Ni_2Cd and Nd_2Ni_2Cd full nickel occupancy was observed from the structure refinements. Nevertheless, small

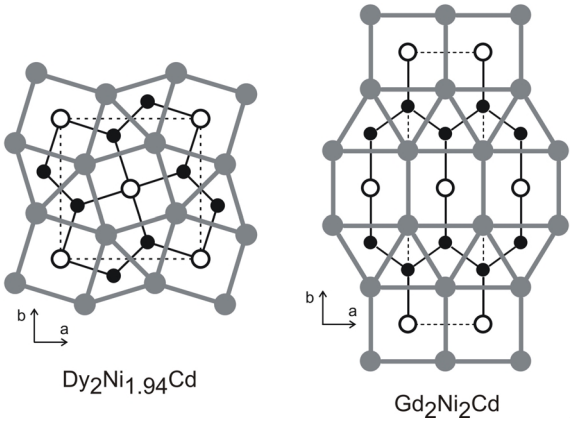

Fig. 1. Projections of the LT-$Dy_2Ni_{1.94}Cd$ and HT-Gd_2Ni_2Cd structures onto the *xy* planes. All atoms lie on mirror planes at $z = 0$ (thin lines) and $z = 1/2$ (thick lines), respectively. The rare earth, nickel, and cadmium atoms are drawn as medium grey, black filled, and open circles, respectively. The two-dimensional $[Ni_2Cd]$ networks and the AlB_2 and CsCl related slabs are emphasized.

nickel defects have been observed for $Sm_2Ni_{1.93}Cd$ and $Dy_2Ni_{1.94}Cd$, while the so far largest defects for Mo_2FeB_2 type compounds [1] were found for $La_2Ni_{1.67}Cd$.

The crystal chemistry of the Mo_2FeB_2 related intermetallics has been described in detail in a recent review [1]. In the following discussion we focus only on the structural relationship with the Mn_2AlB_2 type. As examples we present projections of the tetragonal $Dy_2Ni_{1.94}Cd$ and the orthorhombic Gd_2Ni_2Cd structures along the short unit cell axis in Fig. 1. Both structures are built up from slightly distorted AlB_2 and CsCl related slabs of compositions $RENi_2$, $RENi_{2-x}$, and *RECd*. As pure binary phases, the $RENi_2$ compounds crystallize with the structure of the cubic Laves phase $MgCu_2$, while the high- and low-temperature modifications of the *RE*Cd intermetallics indeed adopt CsCl related arrangements [26]. The tesselation of the AlB_2 and CsCl related slabs is different in both structures. In $Dy_2Ni_{1.94}Cd$ each CsCl slab is condensed with four AlB_2 slabs, while each CsCl slab is attached to two AlB_2 and two CsCl slabs in Gd_2Ni_2Cd. This leads to significant differences for the $[Ni_2Cd]$ networks. The $Dy_2Ni_{1.94}Cd$ structure has only Ni_2 pairs, while infinite Ni–Ni zig-zag chains occur in Gd_2Ni_2Cd. Both nickel substructures are connected *via* the cadmium atoms as emphasized in Fig. 1.

The Ni–Ni distances of 244 pm in the Ni–Ni zig-zag chains of Gd_2Ni_2Cd are shorter than in the Ni_2

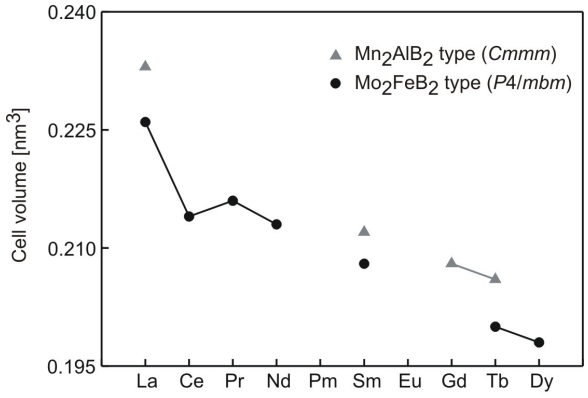

Fig. 2. Plot of the cell volumes of the LT- and HT-RE_2Ni_2Cd intermetallics.

dumb-bells (251 pm) of $Dy_2Ni_{1.94}Cd$. Both Ni–Ni distances are close to the Ni–Ni distance of 249 pm in *fcc* nickel [27], and the Ni–Cd distance of 284 pm is also slightly smaller in Gd_2Ni_2Cd as compared to $Dy_2Ni_{1.94}Cd$ (292 pm). Both distances are significantly longer than the sum of the covalent radii of 257 pm [28]. The cadmium atoms have square-planar nickel coordination in $Dy_2Ni_{1.94}Cd$, but only two nickel neighbors in the [Ni_2Cd] network of Gd_2Ni_2Cd. The two cadmium atoms in the neighboring CsCl slabs are far away (394 pm), and thus Cd–Cd bonding can safely be ruled out, also for $Dy_2Ni_{1.94}Cd$ (366 pm shortest Cd–Cd distance). These Cd–Cd distances are considerably longer than in *hcp* cadmium (6×298 and 6×329 pm) [27]. The smaller Ni–Ni and Ni–Cd distances in Gd_2Ni_2Cd are compensated by longer *RE*–Ni (285 and 298 pm *vs* 281 and 286 pm) and *RE*–Cd distances (333 *vs* 328 pm) as compared to $Dy_2Ni_{1.94}Cd$.

The coordination polyhedra of the rare earth and nickel atoms are similar in both structures. The dysprosium and gadolinium atoms both have coordination number CN = 17 with 6 Ni + 4 Cd + 7 *RE* atoms in their coordination shell. The nickel atoms have CN = 9 in the form of tri-capped trigonal prisms, a typical coordination polyhedron for transition metal atoms in such intermetallics. The capping atoms are 1 Ni + 2 Cd in $Dy_2Ni_{1.94}Cd$ and 2 Ni + 1 Cd in Gd_2Ni_2Cd. As already discussed above, the cadmium atoms in Gd_2Ni_2Cd have only linear nickel coordination, leading to the smaller CN 10. The longer Cd–Cd contacts at 394 pm can only be considered as elements of the coordination polyhedron from a purely geometric point of view (tetra-capped square prism). According to the Goldschmidt rule, the smaller coordination number in the high-temperature form is as expected.

Finally we draw back to the cell volumes of the various RE_2Ni_2Cd intermetallics. These volumes are drawn in Fig. 2 as a function of the rare earth element. For both, the Mo_2FeB_2 and the Mn_2AlB_2 type compounds, the cell volume decreases from the lanthanum to the terbium compound, as expected from the lanthanoid contraction. The cell volumes of the high-temperature forms are about 3% larger than those of the low-temperature ones. $Ce_2Ni_{1.88}Cd$ [2] shows a negative deviation from the smooth curve, due to the intermediate cerium valence, similar to $Ce_2Rh_{1.86}Cd$ [8]. For both compounds, the *a* lattice parameter fits in between that of the lanthanum and the praseodymium compound, while the *c* lattice parameter is even smaller than that of the praseodymium (for $Ce_2Ni_{1.88}Cd$), respectively the neodymium compound. The cerium valence has thus a pronounced influence on the *c* lattice parameter.

Acknowledgements

We thank H.-J. Göcke for the work at the scanning electron microscope. This work was supported by the Deutsche Forschungsgemeinschaft. R.M. is indebted to the Alexander von Humboldt-Stiftung for a research grant.

[1] M. Lukachuk, R. Pöttgen, Z. Kristallogr. **218**, 767 (2003).
[2] D. Niepmann, R. Pöttgen, B. Künnen, G. Kotzyba, J. Solid State Chem. **150**, 139 (2000).
[3] R. Pöttgen, A. Fugmann, R.-D. Hoffmann, U. Ch. Rodewald, D. Niepmann, Z. Naturforsch. **55b**, 155 (2000).
[4] R.-D. Hoffmann, A. Fugmann, U. Ch. Rodewald, R. Pöttgen, Z. Anorg. Allg. Chem. **626**, 1733 (2000).
[5] R. Mishra, R. Pöttgen, R.-D. Hoffmann, D. Kaczorowski, H. Piotrowski, P. Mayer, C. Rosenhahn, B. D. Mosel, Z. Anorg. Allg. Chem. **627**, 1283 (2001).
[6] K. Łątka, R. Kmieć, A. W. Pacyna, R. Mishra, R. Pöttgen, Solid State Sciences **3**, 545 (2001).
[7] R. Mishra, R.-D. Hoffmann, R. Pöttgen, Z. Naturforsch. **56b**, 239 (2001).
[8] F. Stadler, Th. Fickenscher, R. Pöttgen, Z. Naturforsch. **56b**, 1241 (2001).
[9] R. Kraft, Th. Fickenscher, G. Kotzyba, R.-D. Hoffmann, R. Pöttgen, Intermetallics **11**, 111 (2003).
[10] G. Kotzyba, R. Mishra, R. Pöttgen, Z. Naturforsch. **58b**, 497 (2003).
[11] R. Kraft, R. Pöttgen, Monatsh. Chem. **135**, 1327 (2004).

[12] F. Hulliger, B. Z. Xue, J. Alloys Compd. **215**, 267 (1994).
[13] M. Giovannini, H. Michor, E. Bauer, G. Hilscher, P. Rogl, R. Ferro, J. Alloys Compd. **280**, 26 (1998).
[14] D. Kaczorowski, P. Rogl, K. Hiebl, Phys. Rev. B **54**, 9891 (1996).
[15] F. Canepa, S. Cirafici, F. Merlo, M. Pani, C. Ferdeghini, J. Magn. Magn. Mater. **195**, 646 (1999).
[16] W. Rieger, H. Nowotny, F. Benesovsky, Monatsh. Chem. **95**, 1502 (1964).
[17] W. H. Zachariasen, Acta Crystallogr. **2**, 94 (1949).
[18] K. Remschnig, T. Le Bihan, H. Noël, P. Rogl, J. Solid State Chem. **97**, 391 (1992).
[19] H. J. Becher, K. Krogmann, E. Peisker, Z. Anorg. Allg. Chem. **344**, 140 (1996).
[20] R. Pöttgen, Th. Gulden, A. Simon, GIT Labor Fachzeitschrift **43**, 133 (1999).
[21] D. Kußmann, R.-D. Hoffmann, R. Pöttgen, Z. Anorg. Allg. Chem. **624**, 1727 (1998).
[22] K. Yvon, W. Jeitschko, E. Parthé, J. Appl. Crystallogr. **10**, 73 (1977).
[23] G. M. Sheldrick, SHELXL-97, Program for Crystal Structure Refinement, University of Göttingen, Germany (1997).
[24] V. I. Zaremba, V. A. Bruskov, P. Yu. Zavalii, Ya. M. Kalychak, Izv. Akad. Nauk SSSR, Neorg. Mater. **24**, 409 (1988).
[25] Ya. M. Kalychak, V. I. Zaremba, V. M. Baranyak, P. Yu. Zavalii, V. A. Bruskov, L. V. Sysa, O. V. Dmytrakh, Neorg. Mater. **26**, 94 (1990).
[26] P. Villars, L. D. Calvert, Pearson's Handbook of Crystallographic Data for Intermetallic Phases, Second Edition, American Society for Metals, Materials Park, OH 44073 (1991), and desk edition (1997).
[27] J. Donohue, The Structures of the Elements, Wiley, New York (1974).
[28] J. Emsley, The Elements, Oxford University Press, Oxford (1999).